

μ GUIDE: a framework for microstructure imaging via generalized uncertainty-driven inference using deep learning

Maëliss Jallais^{1,2} and Marco Palombo^{1,2}

¹ Cardiff University Brain Research Imaging Centre (CUBRIC), School of Psychology, Cardiff University, Cardiff, United Kingdom;

² School of Computer Science and Informatics, Cardiff University, Cardiff, United Kingdom

January 1, 2024

Abstract

This work proposes μ GUIDE: a general Bayesian framework to estimate posterior distributions of tissue microstructure parameters from any given biophysical model or MRI signal representation, with exemplar demonstration in diffusion-weighted MRI. Harnessing a new deep learning architecture for automatic signal feature selection combined with simulation-based inference and efficient sampling of the posterior distributions, μ GUIDE bypasses the high computational and time cost of conventional Bayesian approaches and does not rely on acquisition constraints to define model-specific summary statistics. The obtained posterior distributions allow to highlight degeneracies present in the model definition and quantify the uncertainty and ambiguity of the estimated parameters.

1 Introduction

Diffusion-weighted MRI (dMRI) is a promising technique for characterizing brain microstructure in-vivo using a paradigm called microstructure imaging [Novikov et al., a, Alexander et al., Jelescu et al., b]. Traditionally, microstructure imaging quantifies histologically meaningful features of brain microstructure by defining a forward (biophysical) model to link the model parameters to measured dMRI signal. These tissue microstructure parameters are then inferred by fitting the biophysical model voxel-wise to the set of signals obtained from images acquired with different sensitivities, yielding model parameter maps [Alexander et al.].

Most commonly used techniques rely on a non-linear curve fitting of the signal and return the optimal solution, i.e. the best parameter guess of the fitting procedure. However, these methods only return one possible combination of tissue parameters that could explain an observed signal and hide model degeneracies, that is all the other possible estimates [Jelescu et al., c]. To address this degeneracy problem, a first approach is to increase the quantity of information contained in the signal that is fed to the fitting procedure by, for example, varying some acquisition parameters such as the echo time [Veraart et al., c] or the diffusion time [Jespersen et al.], using very strong multi-directional diffusion encoding [Veraart et al., a, Olesen et al.] or adding "orthogonal" acquisitions such as double diffusion encoding [Vincent et al.]. However, this solution might not be doable in practice as it leads to longer acquisition times and increased costs. Multiple strategies have therefore been proposed to deal with the degeneracy problem for a given acquisition. Some methods suggest to remove the degeneracy arising from the model definition by imposing additional constraints on the parameters or fixing them to predetermined values [Fieremans et al., a, Zhang et al.]. Nevertheless, the biophysical validity of those constraints remains questionable [Novikov et al., b], potentially introducing bias in pathological tissue evaluations [Novikov et al., a]. Another alternative is optimizing the machine learning training dataset to eliminate degenerate parameter combinations [Guerreri et al.]. Other works propose different strategies for selecting the preferred solution [Novikov et al., b, Fieremans et al., b]. This selection is nontrivial, since the multiple parameter sets often appear equally biophysically plausible. An erroneous choice of parameters can significantly alter the biophysical and diagnostic implications of the estimated parameters. Instead of attempting to remove the degeneracies, we propose to highlight them and present all the possible parameter values that could explain an observed signal.

Another crucial consideration in model fitting is accounting for the uncertainty in parameter estimates. This uncertainty serves various purposes, including assessing result confidence [Jones], quantifying noise effects [Behrens et al.] or assisting in experimental design [Alexander, a]. Gradient descent often provides a measure of confidence for each parameter estimate. Alternative approaches use the shape of the fitted tensor itself as a measure of uncertainty for the fiber direction [Koch et al., Parker and Alexander]. Other methods also rely on bootstrapping techniques to estimate uncertainty. Repetition bootstrapping for example depends on repeated measurements of signal for each gradient direction, but imply a long acquisition time and cost, and are prone to motion artifacts [Lazar and Alexander, Jones]. In contrast, residual bootstrapping methods resample the residuals of a regression model. Yet, this approach is heavily dependent on the model and can easily lead to overfitting [Whitcher et al., Chung et al.]. In general, resampling methods can be problematic for sparse samples, as the bootstrapped samples tend to underestimate the true randomness of the distribution [Kauermann et al.].

Posterior distributions are powerful tools to characterize all the possible parameter estimations that could explain an observed measurement, the uncertainty in those estimations, and existing model degeneracies [Behrens et al.]. Bayesian inference allows for the estimation of these posterior distributions, via the definition of two quantities: the prior distribution, which encodes our initial knowledge of the parameter values ; and the likelihood function of the forward model being studied.

Two main approaches exist to approximate these posterior distributions. Traditional methods rely on the estimation of the likelihood of the observed data point via an analytic expression. The likelihood for most of the models being intractable, these methods are practically unusable [Cranmer et al.]. To circumvent this issue, some techniques have been proposed to sample numerically from the likelihood function, such as Markov-Chain-Monte-Carlo (MCMC) methods [Behrens et al., Alexander, a, Sotiropoulos et al.]. However, the need to call the forward model for each studied sample makes these conventional Bayesian inference methods computationally expensive and time consuming. It also often requires adjustments and tuning specific to each biophysical model, such as the choice of burn-in length, thinning and the number of samples to store. Some open source packages, such as the Microstructure Diffusion Toolbox [Harms and Roebroek], propose a GPU implementation of MCMC with pre-optimized parameters for various models, allowing to reduce the computation time.

The second set of approaches proposes to bypass the estimation of the likelihood distribution and to directly learn the posterior distribution by using a conditional density estimator, allowing to greatly reduce the computation times. These methods are dubbed Likelihood-Free Inference (LFI), or Simulation-Based Inference (SBI) methods. In particular, a growing interest has been observed towards deep generative modeling approaches in the machine learning community. They rely on specially tailored neural network architectures to approximate probability density functions from a set of examples. Normalizing flows [Papamakarios et al., a] are a particular class of such neural networks that have demonstrated promising results for likelihood-free inference in different research fields [Cranmer et al., Gonçalves et al., Greenberg et al.].

A challenge when dealing with data like dMRI is to handle their high-dimensionality. As the dimensionality of the data grows, the complexity of the corresponding inverse problem also increases, leading to longer computation times. To address this issue, recent machine learning methods have been developed to accelerate posterior distribution estimation by relying on the definition of summary statistics [Blum et al., Chen et al.]. These summary statistics are features that capture the essential information within a signal, allowing to reduce the size of the input signal. However, in the dMRI field, these summary statistics are manually designed, model-specific, not easy to define and rely on specific acquisition requirements [Novikov et al., b, Jallais et al.].

Harnessing a new deep learning architecture for automatic signal feature selection and efficient sampling of the posterior distributions, here we propose μ GUIDE: a general Bayesian framework to estimate posterior distributions of tissue microstructure parameters from any given biophysical model/signal representation. μ GUIDE extends and generalises previous work [Jallais et al.] to any forward model and without acquisition constraints, providing fast estimations of posterior distributions voxel-wise. We demonstrate μ GUIDE using numerical simulations on three biophysical models from the literature and compare the obtained estimates with existing methods, including the conventional MCMC approach. We then apply the proposed framework to dMRI data acquired from healthy human volunteers and participants with epilepsy. μ GUIDE framework is agnostic to the origin of the data and the details of the forward model, so we envision its usage and utility to perform Bayesian inference of model parameters also using data from other MRI modalities (e.g. relaxation MRI) and beyond.

2 Theory

2.1 Solving the inverse problem using Bayesian inference

2.1.1 The inference problem

We make the hypothesis that an observed dMRI signal \mathbf{x}_0 can be explained (and generated) using a handful of relevant tissue microstructure parameters $\boldsymbol{\theta}_0$, following the definition of a forward model:

$$\mathbf{x}_0 = \mathcal{M}(\boldsymbol{\theta}_0)$$

The objective is, given this observation \mathbf{x}_0 , to estimate the parameters $\boldsymbol{\theta}_0$ that generated it.

Forward models are designed to mimic at best a given biophysical phenomenon, for some given time and scale [Alexander, b, Yablonskiy and Sukstanskii, Jelescu and Budde, Novikov et al., a, Alexander et al., Jelescu et al., b]. As a consequence, forward models are injection functions (every biologically plausible $\boldsymbol{\theta}_i$ generates exactly one signal \mathbf{x}_i), but do not always happen to be bijections, meaning that multiple $\boldsymbol{\theta}_i$ can generate the same signal \mathbf{x}_i . It can be impossible, based on biological considerations, to infer which solution $\boldsymbol{\theta}_i$ best reflects the probed structure. We refer to these models as 'degenerate models'.

Point estimates algorithms, such as minimum least square or maximum likelihood estimation algorithms, allow to estimate one set of microstructure parameters that could explain an observed signal. In the case of degenerate models, the solution space can be multi-modal and those algorithms will hide possible solutions. When considering real-life acquisitions, i.e. noisy and/or under-sampled acquisitions, one also needs to consider the bias introduced with respect to the forward model, and the resulting variance in the estimates [Jones, Behrens et al.].

We propose a new framework that allows for the estimation of full posterior distributions $p(\boldsymbol{\theta}|\mathbf{x}_0)$, that is all the probable parameters that could represent the underlying tissue, along with an uncertainty measure and the interdependency of parameters. These posteriors can help interpreting the obtained results and make more informed decisions.

2.1.2 The Bayesian formalism.

The posterior distribution can be defined using Bayes' theorem as follows:

$$p(\boldsymbol{\theta}|\mathbf{x}_0) = \frac{p(\mathbf{x}_0|\boldsymbol{\theta}) p(\boldsymbol{\theta})}{p(\mathbf{x}_0)} , \quad (1)$$

where $p(\mathbf{x}_0|\boldsymbol{\theta})$ is the likelihood of the observed data point, $p(\boldsymbol{\theta})$ is the prior distribution defining our initial knowledge of the parameter values, and $p(\mathbf{x}_0)$ is a normalizing constant, commonly referred to as the evidence of the data.

The evidence term is usually very hard to estimate, as it corresponds to all the possible realisations of \mathbf{x}_0 , i.e. $p(\mathbf{x}_0) = \int_{all \mathbf{x}_0} p(\mathbf{x}_0|\boldsymbol{\theta}) p(\boldsymbol{\theta}) d\mathbf{x}_0$. For simplification, methods usually estimate an unnormalized probability density function, i.e.

$$p(\boldsymbol{\theta}|\mathbf{x}_0) \propto p(\mathbf{x}_0|\boldsymbol{\theta})p(\boldsymbol{\theta}) . \quad (2)$$

An analytical expression of the likelihood distribution is often hard to write for data points generated by complex non-linear models, making difficult the use of Equation 2. Models that do not admit a tractable likelihood are called *implicit models* [Diggle and Gratton]. Two approaches have then been developed to allow for the estimation of this posterior distribution: either by approximating the likelihood distribution, or by learning directly the posterior distribution using a conditional density estimator. While this work focuses on the estimate of the posterior distribution using a conditional density estimator, we show a comparison with MCMC, which are commonly used methods in the community. We will therefore introduce this method in the following paragraph.

2.1.3 Estimating the likelihood function.

Well-established approaches for estimating the likelihood function are MCMC methods. These methods rely on a noise model to define the likelihood distribution, such as the Rician [Panagiotaki et al., a] or Offset Gaussian models [Alexander, b]. In this work, we will be using the Microstructure Diffusion Toolbox to perform the MCMC computations [Harms and Roebroeck], which relies on

the Offset Gaussian model. The log-likelihood function is then the following:

$$\log(p(\mathbf{x}_0|\boldsymbol{\theta})) = -\frac{\sum (\mathbf{x}_0 - \sqrt{\mathcal{M}(\boldsymbol{\theta})^2 + \sigma^2})^2}{2\sigma^2} - m \cdot \log(\sigma\sqrt{2\pi}) , \quad (3)$$

where $\mathcal{M}(\boldsymbol{\theta})$ is the signal obtained using the biophysical model, σ is the standard deviation of the Gaussian distributed noise, estimated from the reconstructed magnitude images [Dietrich et al.], and m is the number of observations in the dataset.

MCMC methods allow to obtain posterior distributions using Bayes' formula (Eq. 2) with the previously defined likelihood function (Eq. 3) and some prior distributions, which are usually uniform distributions defined on biologically plausible ranges. They generate a multi-dimensional chain of samples which is guaranteed to converge towards a stationary distribution, which approximates the posterior distribution [Metropolis et al., Hastings].

The need to compute the signal following the forward model at each iteration makes these sampling methods computationally expensive and time consuming. In addition, they require some adjustments specific to each model, such as the choice of burn-in length, thinning and the number of samples to store. Harms and Roebroek recommend to use the Adaptive Metropolis-Within-Gibbs (AMWG) algorithm for sampling dMRI models, initialized with a maximum likelihood estimator obtained from non-linear optimization, with 100 to 200 samples for burn-in and no thinning. The recommended number of samples is model-dependent. Authors recommendations can be found in their paper.

2.1.4 Bypassing the likelihood function.

An alternative method was proposed to overcome the challenges associated with approximating the likelihood function and the limitations of MCMC sampling algorithms. This approach involves directly approximating the posterior distribution by utilizing a conditional density estimator, i.e. a family of conditional probability density function approximators denoted as $q_\phi(\boldsymbol{\theta}|\mathbf{x})$. These approximators are parameterized by ϕ and accept both the parameters $\boldsymbol{\theta}$ and the observation \mathbf{x} as input arguments. Our posterior approximation is then obtained by minimizing its average Kullback-Leibler divergence with respect to the conditional density estimator for different choices of \mathbf{x} , as per [Papamakarios and Murray]:

$$\min_{\phi} \mathcal{L}(\phi) \quad \text{with} \quad \mathcal{L}(\phi) = \mathbb{E}_{\mathbf{x} \sim p(\mathbf{x})} [D_{\text{KL}}(p(\boldsymbol{\theta}|\mathbf{x}) \| q_\phi(\boldsymbol{\theta}|\mathbf{x}))] , \quad (4)$$

which can be rewritten as

$$\begin{aligned} \mathcal{L}(\phi) &= \int D_{\text{KL}}(p(\boldsymbol{\theta}|\mathbf{x}) \| q_\phi(\boldsymbol{\theta}|\mathbf{x})) p(\mathbf{x}) d\mathbf{x} , \\ &= -\iint \log(q_\phi(\boldsymbol{\theta}|\mathbf{x})) p(\boldsymbol{\theta}|\mathbf{x}) p(\mathbf{x}) d\boldsymbol{\theta} d\mathbf{x} + C , \\ &= -\iint \log(q_\phi(\boldsymbol{\theta}|\mathbf{x})) p(\mathbf{x}, \boldsymbol{\theta}) d\boldsymbol{\theta} d\mathbf{x} + C , \\ &= -\mathbb{E}_{(\mathbf{x}, \boldsymbol{\theta}) \sim p(\mathbf{x}, \boldsymbol{\theta})} [\log(q_\phi(\boldsymbol{\theta}|\mathbf{x}))] + C , \end{aligned} \quad (5)$$

where C is a constant that does not depend on ϕ . Note that in practice we consider a N -sample Monte-Carlo approximation of the loss function:

$$\mathcal{L}(\phi) \approx \mathcal{L}^N(\phi) = -\frac{1}{N} \sum_{i=1}^N \log(q_\phi(\boldsymbol{\theta}_i|\mathbf{x}_i)) , \quad (6)$$

where the N data points $(\boldsymbol{\theta}_i, \mathbf{x}_i)$ are sampled from the joint distribution with $\boldsymbol{\theta}_i \sim p(\boldsymbol{\theta})$ and $\mathbf{x}_i \sim p(\mathbf{x}|\boldsymbol{\theta}_i)$. We can then use stochastic gradient descent to obtain a set of parameters ϕ which minimizes \mathcal{L}^N .

If the class of conditional density estimators is sufficiently expressive, it can be demonstrated that the minimizer of Eq. (6) converges to $p(\boldsymbol{\theta}|\mathbf{y})$ when $N \rightarrow \infty$ [Greenberg et al.]. It is worth noting that the parametrization ϕ , obtained at the end of the optimization procedure, serves as an amortized posterior for various choices of \mathbf{x} . Hence, for a particular observation \mathbf{x}_0 , we can simply use $q_\phi(\boldsymbol{\theta}|\mathbf{x}_0)$ as an approximation of $p(\boldsymbol{\theta}|\mathbf{x}_0)$.

3 Methods

3.1 Neural density estimators.

In this study, the Sequential Neural Posterior Estimation (SNPE-C) algorithm [Papamakarios and Murray, Greenberg et al.] is employed to train a neural network that directly approximates the posterior distribution. Thus, sampling from the posterior can be done by sampling from the trained neural network. Neural density estimators have the advantage of providing exact density evaluations, in contrast to Variational Autoencoders (VAE [Kingma and Welling]) or generative adversarial networks (GAN [Goodfellow et al.]), which are better suited for generating synthetic data.

The conditional probability density function approximators used in this project belong to a class of neural networks called normalizing flows [Papamakarios et al., a]. These flows are invertible functions capable of transforming vectors generated from a simple base distribution (e.g. the standard multivariate Gaussian distribution) into an approximation of the true posterior distribution. An autoregressive architecture for normalizing flows is employed, implemented via the Masked Autoregressive Flow (MAF [Papamakarios et al., b]), which is constructed by stacking five Masked Autoencoder for Distribution Estimation models (MADE [Germain et al.]).

3.2 Handling the large dimensionality of the data

As the dimensionality of the input data \mathbf{x} grows, the complexity of the corresponding inverse problem also increases. Accurately characterizing the posterior distributions or estimating the tissue microstructure parameters becomes more challenging. As a consequence, it is often necessary to rely on a set of low-dimensional features (or summary statistics) instead of the raw data for the inference task process [Blum et al., Fearnhead and Prangle, Sisson et al., Papamakarios et al., c, Chen et al.]. Learning a set of sufficient statistics before estimating the posterior distribution makes the inference easier and offers many benefits (see e.g. the Rao-Blackwell theorem).

A follow-up challenge lies in the choice of suitable summary statistics. For well-understood problems and data, it is possible to manually design these features using deterministic functions that condense the information contained in the raw signal into a set of handful summary statistics. Previous works, such as [Novikov et al., b] and [Jallais et al.], have proposed specific summary statistics for two different biophysical models. However, defining these summary statistics is difficult and often requires prior knowledge of the problem at hand. In the context of dMRI, they also rely on acquisition constraints and are model-specific.

In this work, the proposed framework aims to be applicable to any forward model and be as general as possible. We therefore propose to learn the summary statistics from the high-dimensional input signals \mathbf{x} using a neural network. This neural network is referred to as an embedding neural network. The observed signals are fed into the embedding neural network, whose outputs are then passed to the neural density estimator. The parameters of the embedding network are learned together with the parameters of the neural density estimator, leading to the extraction of optimal features that minimize the uncertainty of $p(\boldsymbol{\theta}|\mathbf{x})$. Here, we propose to use a Multi-Layer Perceptron (MLP) with three layers as a summary statistics extractor. The number of features N_f extracted by the MLP can be either defined a priori or determined empirically during training.

The full architecture of the proposed Bayesian framework, dubbed μ GUIDE, is presented in Figure 1.

3.3 Quantifying the confidence in the estimates

To easily visualize the estimated posterior distributions in each voxel, it is necessary to define measures that quantify the best estimates and the associated confidence levels. These measures produce easily interpretable maps for each tissue microstructure parameter. We therefore propose the definition of three quantitative measures, extracted from the estimated posterior distributions.

We start by checking whether a posterior distribution is degenerate, that is if the distribution presents multiple distinct parameter solutions, appearing as multiple local maxima. In such cases, we highlight the corresponding voxel with a red dot on the estimated maps. For non-degenerate posterior distributions, we extract three quantities:

1. The Maximum A Posteriori (MAP), which corresponds to the most likely parameter estimate.
2. An uncertainty measure, which quantifies the dispersion of the 50% most probable samples using the interquartile range, relative to the prior range.

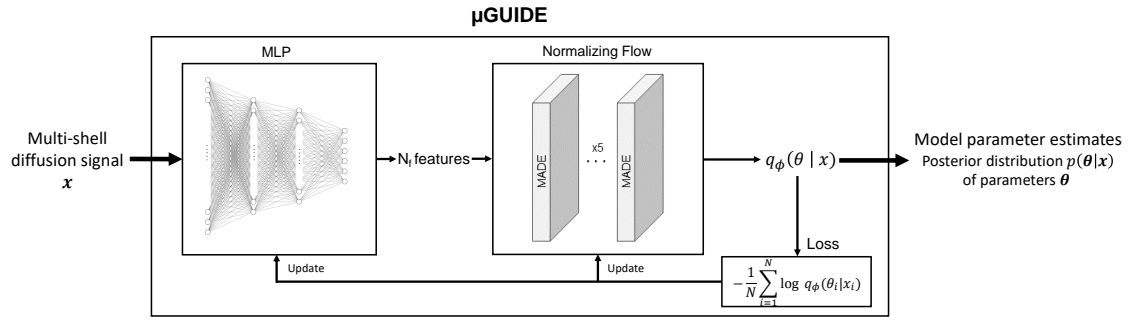


Figure 1: μ GUIDE architecture. Input: an observed signal. Output: a posterior distribution of the model parameters. Based on a SBI framework, it combines a Multi-Layer Perceptron (MLP) with 3 layers and a normalizing flow. The MLP learns a low-dimensional representation of \mathbf{x} , based on a small number of features (N_f), that can be either defined a priori or determined empirically during training. The MLP is trained simultaneously with the normalizing flow, leading to the extraction of the optimal features that minimize the uncertainty of $p(\boldsymbol{\theta}|\mathbf{x})$, i.e. uncertainty-driven.

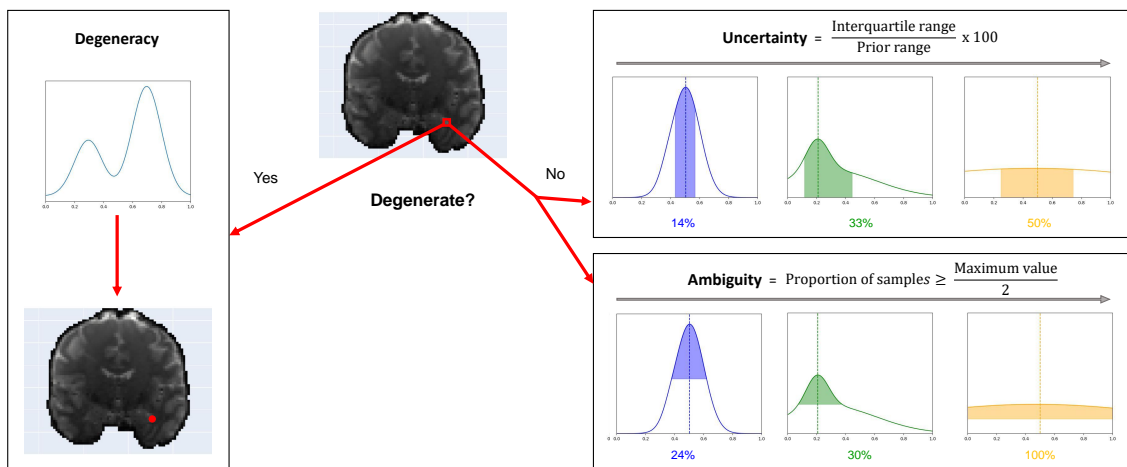


Figure 2: Presentation of the measures introduced to quantify a posterior distribution on exemplar posterior distributions. Maximum A Posteriori (MAP): is the most likely parameter estimate (dashed vertical lines). Degeneracy: highlights the presence of multiple possible parameter solutions in a voxel. Uncertainty: measures the dispersion of the 50% most probable samples using the interquartile range, with respect to the prior range. Ambiguity: measures the Full Width at Half Maximum (FWHM), in percentage with respect to the prior range.

3. An ambiguity measure, which measures the Full Width at Half Maximum (FWHM), in percentage with respect to the prior range.

Figure 2 presents those measures on exemplar posterior distributions.

3.4 Biophysical Models

We show exemplar applications to three biophysical models from the literature with increased complexity. For each model, we compare the fitting quality of the posterior distributions obtained using the MLP and manually defined summary statistics.

- **Model 1: the Ball&Stick model** [Behrens et al.]: This is a two compartment model. The brain tissue is modeled as a stick with diffusivity D_{in} and signal fraction f_{in} , and a ball, with diffusivity D_e . The direction of the stick is randomly sampled on a sphere. This model has the main advantage of being non-degenerate. We define the summary statistics as the direction-averaged signal (seven b-shells, see section 3.6).
- **Model 2: the Standard Model (SM)** [Novikov et al., a]: The microstructure parameters of this two-compartment model are the neurite signal fraction f , the intra-neurite diffusivity D_a , the orientation dispersion index ODI , and the parallel and perpendicular diffusivities within the extra-neurite space D_e^{\parallel} and D_e^{\perp} . We use the LEMONADE [Novikov et al., b]

system of equations, which is based on a cumulant decomposition of the signal, to define six summary statistics.

- **Model 3: an extended-SANDI model** [Palombo et al.]: The parameters of interest of this three-compartment model are the neurite signal fraction f_n , the intra-neurite diffusivity D_n , the orientation dispersion index ODI , soma signal fraction f_s , a proxy of soma radius and diffusivity C_s [Jallais et al.], extra-cellular signal fraction f_e and isotropic diffusivity D_e . We use the six summary statistics defined in [Jallais et al.], which are based on a high and low b-value signal expansion.

Prior distributions $p(\theta)$ are defined as uniform distributions over biophysically plausible ranges. Signal fractions are defined within the interval $[0, 1]$, diffusivities between 0.1 and $3 \mu\text{m}^2 \text{ms}^{-1}$, ODI between 0.03 and 0.95 , and C_s between 0.15 and $1105 \mu\text{m}^2$.

The SM imposes the constraint $D_e^\perp < D_e^\parallel$. To generate samples uniformly distributed on the space defined by this condition, we are using two random variables u_0 and u_1 , both sampled uniformly between 0 and 1 , and then relate them to D_e^\parallel and D_e^\perp using the following equations:

$$\begin{cases} D_e^\parallel = \sqrt{(3.0 - 0.1)^2 \cdot u_0} + 0.1 \\ D_e^\perp = (D_e^\parallel - 0.1) \cdot u_1 + 0.1 \end{cases} \quad (7)$$

The extended SANDI model requires for the signal fractions to sum to 1 , that is $f_n + f_s + f_e = 1$. We define new parameters k_1 and k_2 , uniformly sampled between 0 and 1 , and use the following equations to get the corresponding signal fractions:

$$\begin{cases} f_n = k_2 \sqrt{k_1} \\ f_s = (1 - k_2) \sqrt{k_1} \\ f_e = 1 - \sqrt{k_1} \end{cases} \quad (8)$$

To ensure comparability of results, we extract the same number of features N_f using the MLP as the number of summary statistics for each model. We therefore use $N_f = [7, 6, 6]$ for the Ball&Stick, the SM and the extended-SANDI model, respectively.

3.5 Validation in Numerical Simulations

We start by validating the proposed method by comparing the obtained posterior distributions with a classical method for posterior estimations (MCMC) on the Standard Model. We generated simulations following the same acquisition protocol as the real data (see section 3.6), and added a Rician noise with a Signal-to-Noise Ratio (SNR) of 50 . We then estimated the posterior distributions using both μGUIDE and the MDT toolbox [Harms and Roebroek] to perform the MCMC computations.

We then compared the proposed framework to a state-of-the-art method for posterior estimation [Jallais et al.]. This method relies on manually-defined summary statistics, while μGUIDE automatically extracts some features using an embedded neural network. μGUIDE was trained directly on noisy simulations. The manually-defined summary statistics were extracted from these simulations and then used as training dataset for a MAF, similarly to [Jallais et al.].

At least, we show that μGUIDE can be applicable to any model. While the complexity of the models increase, more degeneracies can be found. The degeneracies are inherent to the model definition, and are not induced by the noise. μGUIDE allows to highlight those degeneracies and quantify the confidence in the obtained estimates.

The training was performed on $N = 10^6$ numerical simulations for each model, computed using the MISST package [Ianus et al.] and random combinations of the model parameters, each uniformly sampled from the previously defined ranges. An open-source package for μGUIDE is available at: <https://github.com/mjallais/uGUIDE>. It relies on the *pyro* [Bingham et al.] package for carrying the probabilistic programming. Both CPU and GPU are supported.

3.6 dMRI Data Acquisition and Processing

We applied μGUIDE to two participants: a healthy volunteer from the MICRA dataset [Koller et al.] and an age-matched participant with epilepsy (FCD Type IIB) ref?. Data were acquired on a Connectome 3T scanner using a PGSE acquisition with b-values = $[200, 500, 1200, 2400, 4000, 6000]$ s mm^{-2} , $[20, 20, 30, 61, 61, 61]$ uniformly distributed directions respectively and 13 non-diffusion-weighted images at 3mm isotropic resolution. TR was set to 3000 ms, TE to 59 ms, and the

diffusion gradient duration and separation to 7 ms and 24 ms respectively. Short diffusion times and TE were achieved thanks to the Connectom gradients, allowing to enhance the signal-to-noise ratio and sensitivity to small water displacements [Jones et al., Setsompop et al.]. We considered the noise as Rician with an SNR of 50 for both subjects.

Data were preprocessed using tools from the FSL [Andersson et al., Andersson and Sotiropoulos] and MRTrix [Veraart et al., b, Vos et al.] software packages. The preprocessing steps included denoising [Veraart et al., b], drift correction [Vos et al.], eddy correction [Andersson and Sotiropoulos], correction for gradient non-linearity distortions [Glasser et al.] with spatio-temporal b-value/vector tracking [Rudrapatna et al.], and Gibbs ringing artefacts correction [Kellner et al.].

3.7 dMRI Data Analysis

Diffusion signals were first normalized by the mean non-diffusion-weighted signals acquired for each voxel. Each voxel was then estimated in parallel using the μ GUIDE framework. For each observed signal \mathbf{x}_v (i.e. for each voxel), we drew 50000 samples via rejection-sampling from $q_\phi(\theta_i|\mathbf{x}_v)$ for each model parameter θ_i , allowing to retrieve the full posterior distributions. We fitted two Gaussian distributions to the obtained posterior distributions to check whether a voxel was considered as degenerate. A voxel is considered as degenerate if the derivative of the fitted Gaussian distributions changes signs more than once (i.e. multiple local maxima), and if the two Gaussian distributions are not overlapping (the distance between the two Gaussian means is inferior to the sum of their standard deviations). If a posterior distribution was not deemed degenerate, the maximum-a-posteriori, uncertainty and ambiguity measures were extracted from the posterior distributions.

The manually-defined summary statistics of the SM are defined using a cumulant expansion, which is only valid for small b-values. We therefore only used the $b \leq 2500$ s mm⁻² data for this model. In a matter of obtaining comparable results, we restricted the application of μ GUIDE to this range of b-values as well. Similarly, an extra b-shell (b-value = 5000 s mm⁻²; 61 directions) was interpolated using *mapl* [Fick et al.] for the extended-SANDI model when using the method developed by Jallais et al. based on summary statistics.

Computations have been performed both on CPU and GPU (NVIDIA GeForce RTX 4090).

4 Results

4.1 Simulations

4.1.1 Comparison with MCMC

We performed a comparison between the posterior distributions obtained using μ GUIDE and MCMC, a classical Bayesian method. Figure 3A shows posterior distributions on two exemplar simulations with SNR = 50 using the SM, obtained with 15000 samples. Sharper and less biased posterior estimations are obtained using μ GUIDE. Figure 3B presents histograms for each model parameter of the bias between the ground truth value used to simulate a signal, and the maximum-a-posteriori of the posterior distributions obtained with either μ GUIDE or MCMC, on 200 simulations. Results indicate that the bias is similar or smaller using μ GUIDE. Overall, μ GUIDE posterior distributions are more accurate than the ones obtained with MCMC.

Moreover, it took on average 32s per simulation to obtain the posterior distribution using MCMC on a GPU, while it only took 0.6s for μ GUIDE on a CPU. μ GUIDE is 55 times faster than MCMC, which makes it more suitable for applying it on large datasets.

4.1.2 The importance of feature selection

Figure 4 shows the maximum-a-posteriori extracted from the posterior distributions versus the ground truth parameters used to generate the diffusion signal with the Ball&Stick, SM and extended-SANDI models. Results are shown on 100 noise-free simulations with random parameter combinations. The orange dots have been obtained using μ GUIDE, that is using a MLP for data reduction and extracting respectively $N_f = [7, 6, 6]$ features in each model. These features are then passed to the normalizing flow for the posterior density estimation. The blue dots are obtained using manually-defined summary statistics, i.e. the direction-averaged signal for the Ball&Stick model, the LEMONADE system of equations for the SM [Novikov et al., b] and the summary statistics defined in [Jallais et al.] for the extended-SANDI model. Less biased MAPs with lower ambiguities and uncertainties are obtained with μ GUIDE, indicating that the MLP allows for the extraction of additional information not contained in the summary statistics, helping to solve the

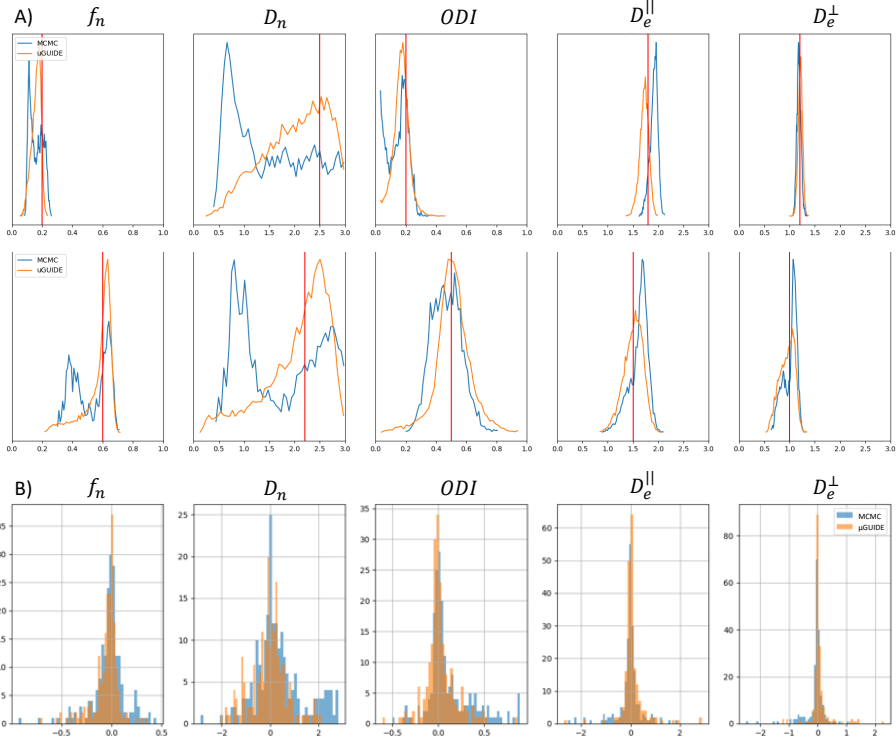


Figure 3: Comparison between μ GUIDE and MCMC. A) Posterior distributions obtained using either μ GUIDE or MCMC on two exemplar simulations with the SM (SNR = 50). B) Bias between the ground truth values used for simulating the diffusion signals, and the maximum-a-posteriori extracted from the posterior distributions using either μ GUIDE or MCMC. Sharper and less biased posterior distributions are obtained using μ GUIDE.

inverse problem. μ GUIDE generalizes the method developed in [Jallais et al.] to make it applicable it to any forward model and any acquisition protocol, while making the estimates more precise and accurate thanks to the automatic feature extraction.

4.1.3 μ GUIDE highlights degeneracies

Figure 5 presents the posterior distributions of microstructure parameters for the Ball&Stick, Standard Model and the extended-SANDI models obtained with μ GUIDE on exemplar noise-free simulations. Blue curves correspond to non-degenerate posterior distributions, while the red ones present at least one degeneracy for one of the parameters. As the complexity of the model increases, degeneracies in the model definitions appear. This figure showcases μ GUIDE ability to highlight those degeneracies in the model parameter estimation. The degeneracies are inherent to the model definition, and are not an artefact generated by noise.

Tables 1 and 2 present the number of degeneracies for each parameter in the three models, on 10000 simulations. Table 1 considers noise-free simulations and the training and estimations were performed on CPU. Table 2 reports results on noisy simulations (Rician noise with SNR = 50), with training and testing performed on a GPU. The time needed for the inference and to estimate the posterior distributions on 10000 simulations, define if they are degenerate or not, and extract the MAP, uncertainty, ambiguity, are also reported.

4.2 Application to real data

After demonstrating that the proposed framework provides good estimates in the case of simulations, we applied μ GUIDE to both a healthy volunteer and a participant with epilepsy. The estimation of the posterior distributions is done independently for each voxel. To easily assess the values and the quality of the fitting, we are plotting the maximum-a-posteriori, ambiguity and uncertainty maps, but the posterior distributions are available for all the voxels. Voxels presenting a degeneracy are highlighted with a red dot.

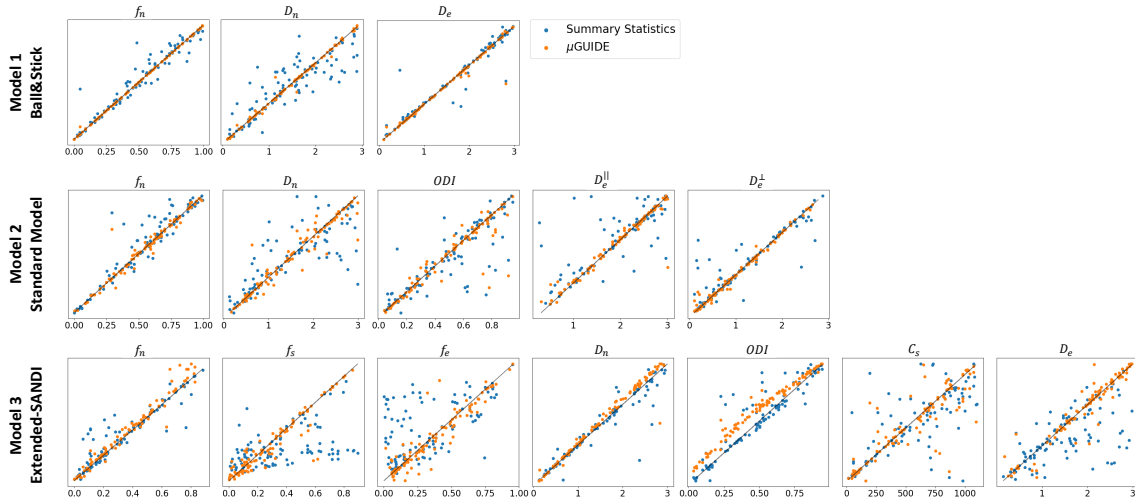


Figure 4: Maximum-A-Posterioris (MAP) extracted from the posterior distributions vs ground truth parameters used for generating the signal for the Ball&Stick, SM and extended SANDI models. Orange points correspond to the MAPs obtained using MLP-extracted features (μ GUIDE) and the blue ones to the MAPs with the manually-defined summary statistics. The summary statistics used in those three models are the direction-averaged signal for the Ball&Stick model, the LEMONADE system of equations [Novikov et al., b] for the SM, and the summary statistics defined in [Jallais et al.] for the extended-SANDI model. Results are shown on 100 exemplar noise-free simulations with random parameter combinations. The optimal features extracted by the MLP allow to reduce the bias and variance of the obtained microstructure posterior distributions.

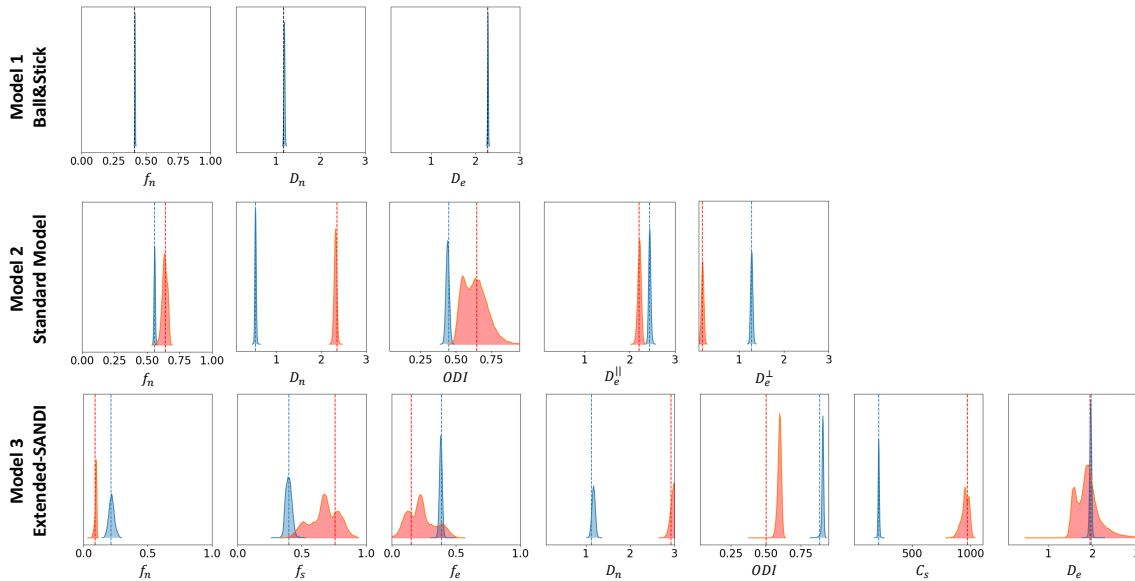


Figure 5: Posterior distributions (diagonal) and joint posterior distributions (upper-diagonal) of the microstructure parameters for the Ball&Stick, SM and extended SANDI models, obtained using μ GUIDE on exemplar noise-free simulations. As the complexity of the model increases, degeneracies appear. μ GUIDE allows to highlight those degeneracies present in the model definition.

Model (SNR = ∞)	Training Time (CPU)	Fitting Time (on 10000 simulations)	Number of Degeneracies (on 10000 simulations)							
			f_n	D_n	$D_e^{ }$	ODI	D_e^{\perp}	f_s	f_e	C_s
Model 1 Ball&Stick	11min	96s	0	0	0	-	-	-	-	-
Model 2 Standard Model	2h02	135s	4	34	23	33	8	-	-	-
Model 3 Extended-SANDI model	2h02	1412s	205	4	260	57	-	1395	2571	1011

Table 1: Number of degeneracies per parameter on 10000 noise-free simulations. Training and estimations of the posterior distributions was performed on CPU. Time for training each model and time for estimating posterior distributions of 10000 noise-free simulations, define if they are degenerate or not, and extract the MAP, uncertainty, ambiguity are also reported.

Model (SNR=50)	Training Time (GPU)	Fitting Time (on 10000 simulations)	Number of Degeneracies (on 10000 simulations)							
			f_n	D_n	D_e^{\parallel}	ODI	D_e^{\perp}	f_s	f_e	C_s
Model 1 Ball&Stick	26min	79s	0	0	0	-	-	-	-	-
Model 2 Standard Model	42min	82s	75	71	117	109	29	-	-	-
Model 3 Extended-SANDI model	50min	238s	47	24	784	6	-	828	1047	56

Table 2: Number of degeneracies per parameter on 10000 noisy simulations (Rician noise with SNR = 50). Training and estimations of the posterior distributions was performed using a GPU. Time for training each model and time for estimating posterior distributions of 10000 noisy simulations, define if they are degenerate or not, and extract the MAP, uncertainty, ambiguity are also reported.

4.2.1 Healthy volunteer

We applied μ GUIDE to a healthy volunteer, using the Ball&Stick, SM and extended-SANDI models. Figure 6 presents the parametric maps of an exemplar set of model parameters for each model, alongside their degeneracy, uncertainty and ambiguity. The Ball&Stick model presents no degeneracies, the SM presents some degeneracies, and the extended-SANDI model a lot more. This result is expected, as the complexity of the models increases, leading to more combinations of tissue parameters that can explain an observed signal. Measures of ambiguity and uncertainty allow to quantify the confidence in the estimates and help interpreting the results.

4.2.2 Participant with epilepsy

Figure 7 demonstrates μ GUIDE application to a participant with epilepsy, using the SM. Noteworthy, the axonal signal fraction estimates within the epileptic lesion show low uncertainty and ambiguity measures hence high confidence, while orientation dispersion index estimates show high uncertainty and ambiguity suggesting low confidence, cautioning the interpretation. The two model parameters also show degeneracy in different regions of the lesion.

5 Discussion

5.1 Applicability of μ GUIDE to multiple models

The μ GUIDE framework offers the advantage of being easily applicable to various biophysical models and representations, thanks to its data-driven approach for data reduction. The need to manually define specific summary statistics that capture the relevant information for microstructure estimation from the multi-shell diffusion signal is removed. This also eliminates the acquisition constraints that were previously imposed by the summary statistics definition. The extracted features contain additional information compared to the summary statistics, resulting in a notable reduction in bias and variance in the estimated posterior distributions. Consequently, μ GUIDE improves parameters estimation over current methods (e.g. Jallais et al.).

In this study, we presented applications of μ GUIDE to brain microstructure estimation using three well-established biophysical models, with increased complexity: the Ball&Stick model, the Standard Model, and an extended-SANDI model. However, our approach is not limited to brain tissue and can be extended to different organs by employing their respective favored models, such as VERDICT in prostate imaging [Panagiotaki et al., b], or even adapted to different imaging modalities. This versatility underscores the broad applicability of our proposed approach across various biological systems and imaging techniques.

It is important to note that μ GUIDE is still a model-dependent method, meaning that the training process is based on the specific model being used. Additionally, the number of features extracted by the MLP needs to be predetermined. One way to determine the number of features is by matching it with the number of parameters being estimated. Alternatively, a dimensionality-reduction study using techniques like tSNE can be conducted to determine the optimal number of features.

5.2 Quantifying confidence to guide interpretation

Quantifying confidence in an estimate is of crucial importance. As demonstrated by our pathological example, changes in the tissue microstructure parameters can help clinicians decide which

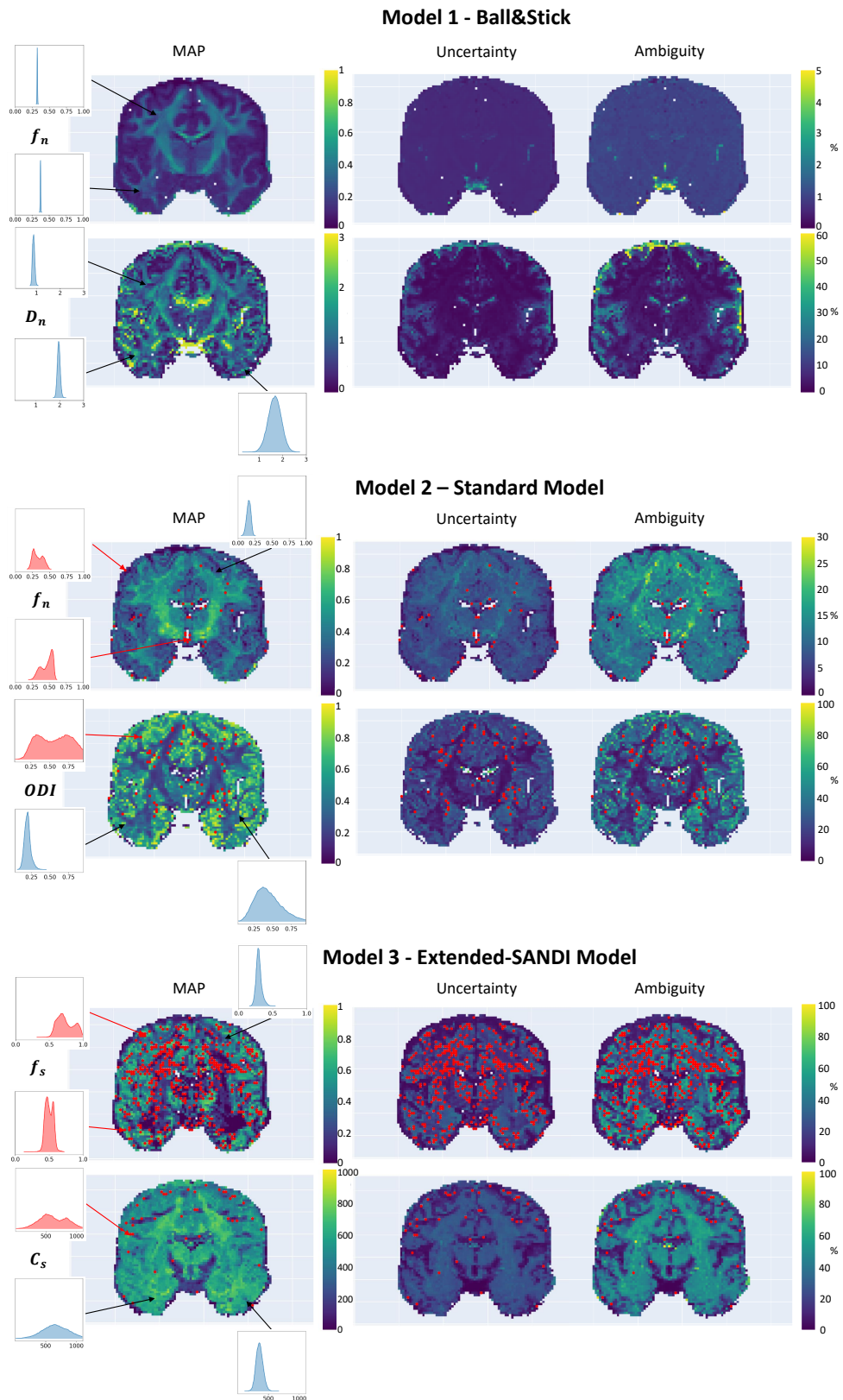


Figure 6: Parametric maps of the Ball&Stick (top), SM (middle) and extended-SANDI model (bottom), obtained using the μ GUIDE framework: maximum-a-posteriori estimation (MAP), uncertainty and ambiguity measures, overlaid with voxels considered degenerate (red dots).

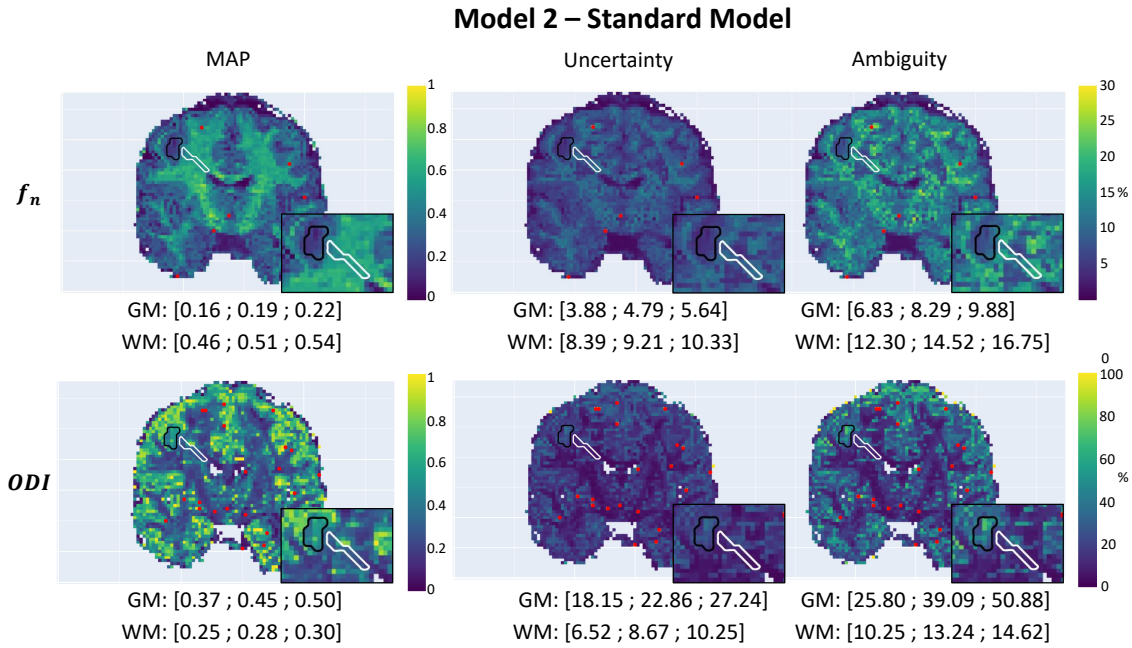


Figure 7: Parametric maps of a participant with epilepsy obtained using the μ GUIDE framework with the SM, superimposed with the grey matter (black) and white matter (white) lesions segmentation. First quartile, mean value and third quartile of the maximum-a-posterior, uncertainty and ambiguity measures are reported in the two regions of interest. Lower MAP values are obtained in the lesions for the axonal signal fraction and the orientation dispersion index compared to healthy tissue. Higher uncertainty and ambiguity ODI values are reported, suggesting less stable estimations.

parameters are the most reliable and better interpret microstructure changes within diseased tissue.

Variance observed in the posterior distributions can be attributed to several factors. The presence of noise in the signal contributes to irreducible variance, decreasing the confidence in the estimates as the noise level increases. Another source of variance can arise from the choice of acquisition parameters. Different acquisitions may provide varying levels of confidence in the parameter estimates. Under-sampled acquisitions or inadequate b-shells may fail to capture essential information about a tissue microstructure, such as soma or neurite radii, resulting in inaccurate estimates. Simulations can guide users in determining whether an acquisition is suitable for estimating parameters of a given model.

Point estimate methods only provide one set of tissue parameters that could explain an observed signal, hiding model degeneracies. To mitigate the issue of degeneracy, several studies have focused on constraining the inverse problem in order to eliminate or minimize degeneracies (e.g. [Fieremans et al. \[a\]](#), [Zhang et al.](#)). One popular approach is NODDI (Neurite Orientation Dispersion and Density Imaging) [[Zhang et al.](#)], which attempts to stabilize the solution by imposing constraints on model parameters. However, those constraints may be not biologically plausible in some conditions [[Novikov et al., b](#)]. As a consequence, a bias may be introduced in the parameter estimation and the inverse problem may remain largely degenerate [[Jelescu et al., c](#)]. We propose instead to highlight the degeneracy via the estimation of the posterior distributions. The user can then make an informed choice and decide on the plausibility of the proposed solutions.

The presence of degeneracy in the solution of the inverse problem is influenced by the complexity of the model being used. In recent years, researchers have introduced increasingly sophisticated models to better represent brain tissue, such as NEXI [[Jelescu et al., a](#)] and eSANDIX [[Olesen et al.](#)], that take into account exchanges between neurites and the extra-cellular space. By applying μ GUIDE, it becomes possible to gain insights into the degree of degeneracy within a model and to assess the balance between model realism and the ability to accurately invert the problem.

5.3 An efficient framework

One notable advantage of the proposed framework is its amortized nature. With this approach, the training process is performed only once, and thereafter, the posterior estimations can be independently obtained for all voxels. This amortization enables efficient estimations of the posterior

distributions. In fact, μ GUIDE outperforms in terms of speed conventional Bayesian inference methods such as MCMC. The time savings achieved with μ GUIDE make it a highly efficient and practical tool for estimating posterior distributions in a timely manner.

6 Conclusion

We proposed a general Bayesian framework, dubbed μ GUIDE, to efficiently estimate posterior distributions of tissue microstructure parameters. For any given acquisition and signal model/representation, μ GUIDE improves parameters estimation over existing methods. It allows to highlight existing degeneracies, and quantify confidence in the estimates, guiding results interpretation.

Acknowledgment

This work, MJ and MP are supported by UKRI Future Leaders Fellowship (MR/T020296/2). We are thankful to Dr. Dmitri Sastin and Dr. Khalid Hamandi for sharing their dataset from a participant with epilepsy.

References

- Daniel C. Alexander. A general framework for experiment design in diffusion MRI and its application in measuring direct tissue-microstructure features. 60(2):439–448, a. ISSN 07403194, 15222594. doi: 10.1002/mrm.21646. URL <https://onlinelibrary.wiley.com/doi/10.1002/mrm.21646>.
- Daniel C. Alexander. Modelling, fitting and sampling in diffusion MRI. In David Laidlaw and Joachim Weickert, editors, *Visualization and Processing of Tensor Fields*, pages 3–20. Springer Berlin Heidelberg, b. ISBN 978-3-540-88377-7 978-3-540-88378-4. doi: 10.1007/978-3-540-88378-4_1. URL http://link.springer.com/10.1007/978-3-540-88378-4_1. Series Title: Mathematics and Visualization.
- Daniel C. Alexander, Tim B. Dyrby, Markus Nilsson, and Hui Zhang. Imaging brain microstructure with diffusion MRI: practicality and applications. 32(4). ISSN 0952-3480, 1099-1492. doi: 10.1002/nbm.3841. URL <https://onlinelibrary.wiley.com/doi/10.1002/nbm.3841>.
- Jesper L.R. Andersson and Stamatios N. Sotiropoulos. An integrated approach to correction for off-resonance effects and subject movement in diffusion MR imaging. 125:1063–1078. ISSN 10538119. doi: 10.1016/j.neuroimage.2015.10.019. URL <https://linkinghub.elsevier.com/retrieve/pii/S1053811915009209>.
- Jesper L.R. Andersson, Stefan Skare, and John Ashburner. How to correct susceptibility distortions in spin-echo echo-planar images: application to diffusion tensor imaging. 20(2):870–888. ISSN 10538119. doi: 10.1016/S1053-8119(03)00336-7. URL <https://linkinghub.elsevier.com/retrieve/pii/S1053811903003367>.
- T.E.J. Behrens, M.W. Woolrich, M. Jenkinson, H. Johansen-Berg, R.G. Nunes, S. Clare, P.M. Matthews, J.M. Brady, and S.M. Smith. Characterization and propagation of uncertainty in diffusion-weighted MR imaging. 50(5):1077–1088. ISSN 0740-3194, 1522-2594. doi: 10.1002/mrm.10609. URL <http://doi.wiley.com/10.1002/mrm.10609>.
- Eli Bingham, Jonathan P. Chen, Martin Jankowiak, Fritz Obermeyer, Neeraj Pradhan, Theofanis Karaletsos, Rohit Singh, Paul Szerlip, Paul Horsfall, and Noah D. Goodman. Pyro: Deep universal probabilistic programming.
- M. G. B. Blum, M. A. Nunes, D. Prangle, and S. A. Sisson. A comparative review of dimension reduction methods in approximate bayesian computation. 28(2). ISSN 0883-4237. doi: 10.1214/12-STS406. URL <https://projecteuclid.org/journals/statistical-science/volume-28/issue-2/A-Comparative-Review-of-Dimension-Reduction-Methods-in-Approximate-Bayesian/10.1214/12-STS406.full>.
- Yanzhi Chen, Michael U Gutmann, and Adrian Weller. Is learning summary statistics necessary for likelihood-free inference?

- SungWon Chung, Ying Lu, and Roland G. Henry. Comparison of bootstrap approaches for estimation of uncertainties of DTI parameters. 33(2):531–541. ISSN 10538119. doi: 10.1016/j.neuroimage.2006.07.001. URL <https://linkinghub.elsevier.com/retrieve/pii/S1053811906007403>.
- Kyle Cranmer, Johann Brehmer, and Gilles Louppe. The frontier of simulation-based inference. page 201912789. ISSN 0027-8424, 1091-6490. doi: 10.1073/pnas.1912789117. URL <http://www.pnas.org/lookup/doi/10.1073/pnas.1912789117>.
- Olaf Dietrich, José G. Raya, Scott B. Reeder, Maximilian F. Reiser, and Stefan O. Schoenberg. Measurement of signal-to-noise ratios in MR images: Influence of multichannel coils, parallel imaging, and reconstruction filters. 26(2):375–385. ISSN 10531807, 15222586. doi: 10.1002/jmri.20969. URL <https://onlinelibrary.wiley.com/doi/10.1002/jmri.20969>.
- Peter J. Diggle and Richard J. Gratton. Monte carlo methods of inference for implicit statistical models. 46(2):193–212. ISSN 00359246. doi: 10.1111/j.2517-6161.1984.tb01290.x. URL <https://onlinelibrary.wiley.com/doi/10.1111/j.2517-6161.1984.tb01290.x>.
- Paul Fearnhead and Dennis Prangle. Constructing summary statistics for approximate bayesian computation: Semi-automatic approximate bayesian computation. 74(3):419–474. ISSN 1369-7412, 1467-9868. doi: 10.1111/j.1467-9868.2011.01010.x. URL <https://academic.oup.com/jrsssb/article/74/3/419/7075312>.
- Rutger H.J. Fick, Demian Wassermann, Emmanuel Caruyer, and Rachid Deriche. MAPL: Tissue microstructure estimation using laplacian-regularized MAP-MRI and its application to HCP data. 134:365–385. ISSN 10538119. doi: 10.1016/j.neuroimage.2016.03.046. URL <https://linkinghub.elsevier.com/retrieve/pii/S1053811916002512>.
- Els Fieremans, Jens H. Jensen, and Joseph A. Helpert. White matter characterization with diffusional kurtosis imaging. 58(1):177–188, a. ISSN 10538119. doi: 10.1016/j.neuroimage.2011.06.006. URL <https://linkinghub.elsevier.com/retrieve/pii/S1053811911006148>.
- Els Fieremans, Dmitry S. Novikov, Jens H. Jensen, and Joseph A. Helpert. Monte carlo study of a two-compartment exchange model of diffusion. 23(7):711–724, b. ISSN 09523480. doi: 10.1002/nbm.1577. URL <https://onlinelibrary.wiley.com/doi/10.1002/nbm.1577>.
- Mathieu Germain, Karol Gregor, Iain Murray, and Hugo Larochelle. MADE: Masked autoencoder for distribution estimation. page 9.
- Matthew F. Glasser, Stamatios N. Sotiropoulos, J. Anthony Wilson, Timothy S. Coalson, Bruce Fischl, Jesper L. Andersson, Junqian Xu, Saad Jbabdi, Matthew Webster, Jonathan R. Polimeni, David C. Van Essen, and Mark Jenkinson. The minimal preprocessing pipelines for the human connectome project. 80:105–124. ISSN 10538119. doi: 10.1016/j.neuroimage.2013.04.127. URL <https://linkinghub.elsevier.com/retrieve/pii/S1053811913005053>.
- Pedro J Gonçalves, Jan-Matthis Lueckmann, Michael Deistler, Marcel Nonnenmacher, Kaan Öcal, Giacomo Bassetto, Chaitanya Chintaluri, William F Podlaski, Sara A Haddad, Tim P Vogels, David S Greenberg, and Jakob H Macke. Training deep neural density estimators to identify mechanistic models of neural dynamics. 9:e56261. ISSN 2050-084X. doi: 10.7554/eLife.56261. URL <https://elifesciences.org/articles/56261>.
- Ian J. Goodfellow, Jean Pouget-Abadie, Mehdi Mirza, Bing Xu, David Warde-Farley, Sherjil Ozair, Aaron Courville, and Yoshua Bengio. Generative adversarial networks. URL <http://arxiv.org/abs/1406.2661>.
- David S. Greenberg, Marcel Nonnenmacher, and Jakob H. Macke. Automatic posterior transformation for likelihood-free inference. URL <http://arxiv.org/abs/1905.07488>.
- Michele Guerreri, Sean Epstein, Hojjat Azadbakht, and Hui Zhang. Resolving quantitative MRI model degeneracy with machine learning via training data distribution design. URL <http://arxiv.org/abs/2303.05464>.
- Robbert L. Harms and Alard Roebroek. Robust and fast markov chain monte carlo sampling of diffusion MRI microstructure models. 12:97. ISSN 1662-5196. doi: 10.3389/fninf.2018.00097. URL <https://www.frontiersin.org/article/10.3389/fninf.2018.00097/full>.

- W. K. Hastings. Monte carlo sampling methods using markov chains and their applications. 57(1):97–109. ISSN 0006-3444. doi: 10.1093/biomet/57.1.97. URL <https://doi.org/10.1093/biomet/57.1.97>. eprint: <https://academic.oup.com/biomet/article-pdf/57/1/97/23940249/57-1-97.pdf>.
- Andrada Ianuș, Noam Shemesh, Daniel C. Alexander, and Ivana Drobnjak. Double oscillating diffusion encoding and sensitivity to microscopic anisotropy: Double oscillating diffusion encoding. 78(2):550–564. ISSN 07403194. doi: 10.1002/mrm.26393. URL <https://onlinelibrary.wiley.com/doi/10.1002/mrm.26393>.
- Maëliss Jallais, Pedro Luiz Coelho Rodrigues, Alexandre Gramfort, and Demian Wassermann. Inverting brain grey matter models with likelihood-free inference: a tool for trustable cytoarchitecture measurements. URL <http://arxiv.org/abs/2111.08693>.
- Ileana O. Jelescu and Matthew D. Budde. Design and validation of diffusion MRI models of white matter. 5. ISSN 2296-424X. doi: 10.3389/fphy.2017.00061. URL <http://journal.frontiersin.org/article/10.3389/fphy.2017.00061/full>.
- Ileana O. Jelescu, Alexandre de Skowronski, Françoise Geffroy, Marco Palombo, and Dmitry S. Novikov. Neurite exchange imaging (NEXI): A minimal model of diffusion in gray matter with inter-compartment water exchange. 256:119277, a. ISSN 10538119. doi: 10.1016/j.neuroimage.2022.119277. URL <https://linkinghub.elsevier.com/retrieve/pii/S1053811922003986>.
- Ileana O. Jelescu, Marco Palombo, Francesca Bagnato, and Kurt G. Schilling. Challenges for biophysical modeling of microstructure. 344:108861, b. ISSN 01650270. doi: 10.1016/j.jneumeth.2020.108861. URL <https://linkinghub.elsevier.com/retrieve/pii/S0165027020302843>.
- Ileana O. Jelescu, Jelle Veraart, Els Fieremans, and Dmitry S. Novikov. Degeneracy in model parameter estimation for multi-compartmental diffusion in neuronal tissue: Degeneracy in model parameter estimation of diffusion in neural tissue. 29(1):33–47, c. ISSN 09523480. doi: 10.1002/nbm.3450. URL <http://doi.wiley.com/10.1002/nbm.3450>.
- Sune Nørhøj Jespersen, Jonas Lyng Olesen, Brian Hansen, and Noam Shemesh. Diffusion time dependence of microstructural parameters in fixed spinal cord. 182:329–342. ISSN 10538119. doi: 10.1016/j.neuroimage.2017.08.039. URL <https://linkinghub.elsevier.com/retrieve/pii/S1053811917306869>.
- Derek K. Jones. Determining and visualizing uncertainty in estimates of fiber orientation from diffusion tensor MRI. 49(1):7–12. ISSN 0740-3194, 1522-2594. doi: 10.1002/mrm.10331. URL <http://doi.wiley.com/10.1002/mrm.10331>.
- D.K. Jones, D.C. Alexander, R. Bowtell, M. Cercignani, F. Dell’Acqua, D.J. McHugh, K.L. Miller, M. Palombo, G.J.M. Parker, U.S. Rudrapatna, and C.M.W. Tax. Microstructural imaging of the human brain with a ‘super-scanner’: 10 key advantages of ultra-strong gradients for diffusion MRI. 182:8–38. ISSN 10538119. doi: 10.1016/j.neuroimage.2018.05.047. URL <https://linkinghub.elsevier.com/retrieve/pii/S1053811918304610>.
- Göran Kauermann, Gerda Claeskens, and J. D. Opsomer. Bootstrapping for penalized spline regression. 18(1):126–146. ISSN 1061-8600, 1537-2715. doi: 10.1198/jcgs.2009.0008. URL <http://www.tandfonline.com/doi/abs/10.1198/jcgs.2009.0008>.
- Elias Kellner, Bibek Dhital, Valerij G. Kiselev, and Marco Reisert. Gibbs-ringing artifact removal based on local subvoxel-shifts. 76(5):1574–1581. doi: <https://doi.org/10.1002/mrm.26054>. URL <https://onlinelibrary.wiley.com/doi/abs/10.1002/mrm.26054>. eprint: <https://onlinelibrary.wiley.com/doi/pdf/10.1002/mrm.26054>.
- Diederik P. Kingma and Max Welling. An introduction to variational autoencoders. In *Foundations and Trends® in Machine Learning*, volume 12, pages 307–392. now Publishers Inc. doi: 10.1561/22000000056.
- Martin A. Koch, David G. Norris, and Margret Hund-Georgiadis. An investigation of functional and anatomical connectivity using magnetic resonance imaging. 16(1):241–250. ISSN 10538119. doi: 10.1006/nimg.2001.1052. URL <https://linkinghub.elsevier.com/retrieve/pii/S1053811901910523>.

- Kristin Koller, Umesh Rudrapatna, Maxime Chamberland, Erika P. Raven, Greg D. Parker, Chantal M.W. Tax, Mark Drakesmith, Fabrizio Fasano, David Owen, Garin Hughes, Cyril Charon, C John Evans, and Derek K. Jones. MICRA: Microstructural image compilation with repeated acquisitions. 225:117406. ISSN 10538119. doi: 10.1016/j.neuroimage.2020.117406. URL <https://linkinghub.elsevier.com/retrieve/pii/S1053811920308910>.
- Mariana Lazar and Andrew L. Alexander. Bootstrap white matter tractography (BOOT-TRAC). 24(2):524–532. ISSN 10538119. doi: 10.1016/j.neuroimage.2004.08.050. URL <https://linkinghub.elsevier.com/retrieve/pii/S1053811904005130>.
- Nicholas Metropolis, Arianna W. Rosenbluth, Marshall N. Rosenbluth, Augusta H. Teller, and Edward Teller. Equation of state calculations by fast computing machines. 21(6):1087–1092. ISSN 0021-9606. doi: 10.1063/1.1699114. URL <https://doi.org/10.1063/1.1699114>. eprint: https://pubs.aip.org/aip/jcp/article-pdf/21/6/1087/8115285/1087_1_online.pdf.
- Dmitry S. Novikov, Els Fieremans, Sune N. Jespersen, and Valerij G. Kiselev. Quantifying brain microstructure with diffusion MRI: Theory and parameter estimation: Brain microstructure with dMRI: Theory and parameter estimation. page e3998, a. ISSN 09523480. doi: 10.1002/nbm.3998. URL <http://doi.wiley.com/10.1002/nbm.3998>.
- Dmitry S. Novikov, Jelle Veraart, Ileana O. Jelescu, and Els Fieremans. Rotationally-invariant mapping of scalar and orientational metrics of neuronal microstructure with diffusion MRI. 174: 518–538, b. ISSN 10538119. doi: 10.1016/j.neuroimage.2018.03.006. URL <https://linkinghub.elsevier.com/retrieve/pii/S1053811918301915>.
- Jonas L. Olesen, Leif Østergaard, Noam Shemesh, and Sune N. Jespersen. Diffusion time dependence, power-law scaling, and exchange in gray matter. 251:118976. ISSN 10538119. doi: 10.1016/j.neuroimage.2022.118976. URL <https://linkinghub.elsevier.com/retrieve/pii/S1053811922001057>.
- Marco Palombo, Andrada Ianus, Michele Guerreri, Daniel Nunes, Daniel C. Alexander, Noam Shemesh, and Hui Zhang. SANDI: A compartment-based model for non-invasive apparent soma and neurite imaging by diffusion MRI. 215:116835. ISSN 10538119. doi: 10.1016/j.neuroimage.2020.116835. URL <https://linkinghub.elsevier.com/retrieve/pii/S1053811920303220>.
- Eleftheria Panagiotaki, Torben Schneider, Bernard Siow, Matt G. Hall, Mark F. Lythgoe, and Daniel C. Alexander. Compartment models of the diffusion MR signal in brain white matter: A taxonomy and comparison. 59(3):2241–2254, a. ISSN 10538119. doi: 10.1016/j.neuroimage.2011.09.081. URL <https://linkinghub.elsevier.com/retrieve/pii/S1053811911011566>.
- Eleftheria Panagiotaki, Simon Walker-Samuel, Bernard Siow, S. Peter Johnson, Vineeth Rajkumar, R. Barbara Pedley, Mark F. Lythgoe, and Daniel C. Alexander. Noninvasive quantification of solid tumor microstructure using VERDICT MRI. 74(7):1902–1912, b. ISSN 0008-5472, 1538-7445. doi: 10.1158/0008-5472.CAN-13-2511. URL <https://aacrjournals.org/cancerres/article/74/7/1902/599821/Noninvasive-Quantification-of-Solid-Tumor>.
- George Papamakarios and Iain Murray. Fast -free inference of simulation models with bayesian conditional density estimation.
- George Papamakarios, Eric Nalisnick, Danilo Jimenez Rezende, Shakir Mohamed, and Balaji Lakshminarayanan. Normalizing flows for probabilistic modeling and inference. a. URL <http://arxiv.org/abs/1912.02762>.
- George Papamakarios, Theo Pavlakou, and Iain Murray. Masked autoregressive flow for density estimation. b. URL <http://arxiv.org/abs/1705.07057>.
- George Papamakarios, David C Sterratt, and Iain Murray. Sequential neural likelihood: Fast likelihood-free inference with autoregressive flows. c.
- Geoff J. M. Parker and Daniel C. Alexander. Probabilistic monte carlo based mapping of cerebral connections utilising whole-brain crossing fibre information. In Chris Taylor and J. Alison Noble, editors, *Information Processing in Medical Imaging*, volume 2732, pages 684–695. Springer Berlin Heidelberg. ISBN 978-3-540-40560-3 978-3-540-45087-0. doi: 10.1007/978-3-540-45087-0_57. URL http://link.springer.com/10.1007/978-3-540-45087-0_57. Series Title: Lecture Notes in Computer Science.

- Umesh Rudrapatna, Greg D. Parker, Jamie Roberts, and Derek K. Jones. A comparative study of gradient nonlinearity correction strategies for processing diffusion data obtained with ultra-strong gradient MRI scanners. 85(2):1104–1113. ISSN 0740-3194, 1522-2594. doi: 10.1002/mrm.28464. URL <https://onlinelibrary.wiley.com/doi/10.1002/mrm.28464>.
- K. Setsompop, R. Kimmlingen, E. Eberlein, T. Witzel, J. Cohen-Adad, J.A. McNab, B. Keil, M.D. Tisdall, P. Hoecht, P. Dietz, S.F. Cauley, V. Tountcheva, V. Matschl, V.H. Lenz, K. Heberlein, A. Potthast, H. Thein, J. Van Horn, A. Toga, F. Schmitt, D. Lehne, B.R. Rosen, V. Wedeen, and L.L. Wald. Pushing the limits of in vivo diffusion MRI for the human connectome project. 80: 220–233. ISSN 10538119. doi: 10.1016/j.neuroimage.2013.05.078. URL <https://linkinghub.elsevier.com/retrieve/pii/S1053811913005788>.
- S. A. Sisson, Y. Fan, and M. A. Beaumont. Overview of approximate bayesian computation. URL <http://arxiv.org/abs/1802.09720>.
- S. N. Sotiropoulos, S. Jbabdi, J. L. Andersson, M. W. Woolrich, K. Ugurbil, and T. E. J. Behrens. RubiX: Combining spatial resolutions for bayesian inference of crossing fibers in diffusion MRI. 32(6):969–982. ISSN 0278-0062, 1558-254X. doi: 10.1109/TMI.2012.2231873. URL <http://ieeexplore.ieee.org/document/6420959/>.
- Jelle Veraart, Els Fieremans, and Dmitry S. Novikov. On the scaling behavior of water diffusion in human brain white matter. 185:379–387, a. ISSN 10538119. doi: 10.1016/j.neuroimage.2018.09.075. URL <https://linkinghub.elsevier.com/retrieve/pii/S1053811918319475>.
- Jelle Veraart, Dmitry S. Novikov, Daan Christiaens, Benjamin Ades-aron, Jan Sijbers, and Els Fieremans. Denoising of diffusion MRI using random matrix theory. 142:394–406, b. ISSN 10538119. doi: 10.1016/j.neuroimage.2016.08.016. URL <https://linkinghub.elsevier.com/retrieve/pii/S1053811916303949>.
- Jelle Veraart, Dmitry S. Novikov, and Els Fieremans. TE dependent diffusion imaging (TEddi) distinguishes between compartmental t2 relaxation times. 182:360–369, c. ISSN 10538119. doi: 10.1016/j.neuroimage.2017.09.030. URL <https://linkinghub.elsevier.com/retrieve/pii/S1053811917307784>.
- Mélissa Vincent, Marco Palombo, and Julien Valette. Revisiting double diffusion encoding MRS in the mouse brain at 11.7t: Which microstructural features are we sensitive to? 207:116399. ISSN 10538119. doi: 10.1016/j.neuroimage.2019.116399. URL <https://linkinghub.elsevier.com/retrieve/pii/S1053811919309905>.
- Sjoerd B. Vos, Chantal M. W. Tax, Peter R. Luijten, Sebastien Ourselin, Alexander Leemans, and Martijn Froeling. The importance of correcting for signal drift in diffusion MRI. 77(1):285–299. ISSN 0740-3194, 1522-2594. doi: 10.1002/mrm.26124. URL <https://onlinelibrary.wiley.com/doi/10.1002/mrm.26124>.
- Brandon Whitcher, David S. Tuch, Jonathan J. Wisco, A. Gregory Sorensen, and Liqun Wang. Using the wild bootstrap to quantify uncertainty in diffusion tensor imaging. 29(3):346–362. ISSN 10659471, 10970193. doi: 10.1002/hbm.20395. URL <https://onlinelibrary.wiley.com/doi/10.1002/hbm.20395>.
- Dmitriy A. Yablonskiy and Alexander L. Sukstanskii. Theoretical models of the diffusion weighted MR signal. 23(7):661–681. ISSN 09523480. doi: 10.1002/nbm.1520. URL <http://doi.wiley.com/10.1002/nbm.1520>.
- Hui Zhang, Torben Schneider, Claudia A. Wheeler-Kingshott, and Daniel C. Alexander. NODDI: Practical in vivo neurite orientation dispersion and density imaging of the human brain. 61(4): 1000–1016. ISSN 10538119. doi: 10.1016/j.neuroimage.2012.03.072. URL <https://linkinghub.elsevier.com/retrieve/pii/S1053811912003539>.